Submitted to the
EPS-HEP2007, 2007 Europhysics Conference on High Energy Physics
July 19-25, 2007, Manchester, England

Abstract: 62 **Session: Strong Interactions**

Measurement of dijet cross sections for events with a leading neutron in photoproduction at HERA

ZEUS Collaboration

Abstract

Differential cross sections for dijet photoproduction in association with a leading neutron in the reaction $e^{+}+p \rightarrow e^{+}+n+\mathrm{jet}+\mathrm{jet}+X$ have been measured with the ZEUS detector at HERA using an integrated luminosity of 40 pb^{-1}. The cross sections were measured for jet transverse energies $E_T^{\mathrm{jet\ 1(jet\ 2)}} > 7.5(6.5)$ GeV, and pseudorapidity $-1.5 < \eta^{\mathrm{jet}} < 2.5$, photon-proton center-of-mass energy $130 < W < 280\,\mathrm{GeV}$, neutron energy $E_n > 184\,\mathrm{GeV}$, and neutron production angle $\theta_n < 0.75$ mrad. The ratio of dijet events with a leading neutron in the final state to the inclusive dijet photoproduction was studied as a function of the jet kinematic variables and W and x_γ, the fraction of the photon energy participating in the hard scattering. The data are broadly consistent with factorization of the lepton and hadron vertices and with a simple one-pion-exchange model. The energy spectra and angular distribution of the neutrons were also measured, and the data compared with recent leading neutron data in deep inelastic scattering; no clear effects of absorption were observed in the data.

1 Introduction

Events with baryons carrying a large fraction of the proton beam energy, $x_L = E_B/E_p$, have been observed in ep scattering at HERA [1–7]. Such processes are of interest because the underlying production mechanisms are not well understood. Leading baryons are produced at a soft scale and purely perturbative techniques do not apply. Different phenomenological approaches were developed to model their production [8–12]. In particular for the leading neutron production studied here, exchanges of isovector mesons, especially pion exchange, have been explored as possible production mechanisms [13, 14].

The results presented in this paper complement earlier studies [4, 7] which focused on the momentum and p_T spectra of leading neutrons and their dependence on kinematic variables in photoproduction and deep inelastic scattering (DIS) with large values of exchanged photon virtuality, $Q^2 > 2\,\mathrm{GeV}^2$. Here these studies are extended to the case of photoproduction of dijets with large transverse energies, E_T. A diagram of this process, with leading neutron production via meson exchange, is show in Fig. 1.

Here are reported cross sections of both inclusive, i.e. no neutron requirement, and neutron tagged photoproduced dijets, and the fraction of neutron tagged events. The tagged neutrons are in the kinematic region $x_L > 0.2$ and $p_T^2 < 0.476\,x_L^2\,\mathrm{GeV}^2$. The photon virtualty is restricted to $Q^2 < 1\,\mathrm{GeV}^2$. The largest (second largest) E_T jets have E_T greater than 7.5 (6.5) GeV. The jets are restricted to the lab frame pseudorapidity range $-1.5 < \eta < 2.5$, and the photon-proton center of mass energy is in the range $130 < W < 280\,\mathrm{GeV}$. The cross sections and ratios are presented as functions of E_T, η, W, and also x_γ, the fraction of the photon energy participating in the hard scattering. The cross sections and ratios are compared to LO and NLO perturbative QCD calculations of Klasen and Kramer [15]. The x_L and p_T^2 distributions are compared to recent results in DIS [7].

2 Jet cross sections and ratios

The dijet photoproduction cross sections and its neutron tagged subsample cross sections are presented in the top of Figs. 2 and 3 as a function of E_T, η, x_γ and W. Statistical and uncorrelated systematic uncertainties are summed in quadrature. The calorimeter energy scale uncertainty is displayed separately as a yellow band. The cross sections for the two samples are similar in shape, the leading neutron cross section being approximately 7% of the inclusive in magnitude.

The comparison between the two samples is best presented in the form of ratios of neutron-tagged to inclusive cross-sections, where most of the systematic effects cancel out. This quantity is shown in the bottom of Figs. 2 and 3 and compared to the LO and NLO predictions from the calculation of Klasen and Kramer [15]. The effects of hadronization corrections to the calculations are expected to largely cancel out in the ratio. In the calculation, leading neutrons are produced via pion-exchange. The cross section is computed assuming Regge factorization, i.e. it is written as the product of a function describing the splitting of a proton into a π-n system, which is the pion flux factor $f_{\pi/p}(x_L,t)$, and the hard cross section $\hat{\sigma}_{\gamma\pi}$ involving the pion structure function. The pion flux factor is parametrized as [16]:

$$f_{\pi/p}(x_L,t) = \frac{1}{4\pi}\frac{2g^2_{p\pi p}}{4\pi}\frac{-t}{(t-m^2_\pi)^2}(1-x_L)^{1-2\alpha(t)}\left[F(x_L,t)\right]^2, \tag{1}$$

with the form factor of [16]

$$F(x_L,t) = \exp\left[R^2\frac{(t-m^2_\pi)}{(1-x_L)}\right], \;\; \alpha(t)=0. \tag{2}$$

The parameter R was set to $R = 0.65\,\mathrm{GeV}^{-1}$ for LO calculations and $R = 0.55\,\mathrm{GeV}^{-1}$ for NLO calculations.

The strong rise of the ratio as a function of x_γ, in Fig. 3, closely related to the milder decrease in the ratio as a funcion of η, in Fig. 2, is mainly due to kinematic effects, and is reasonably well described by the NLO calculation. The prediction of LO is somewhat flatter than the data. The ratios as a function of E_T and W are flat and in agreement with NLO predictions. All results are consistent with the Regge factorization hypothesis.

Figure 4 shows the normalized differential distribution $(1/\sigma_{\mathrm{inc}})d\sigma_{\mathrm{LN}}/dx_L$ for neutrons with scattering angles $\theta_n < 0.75\,\mathrm{mrad}$, corresponding to the kinematic range $p_T^2 < 0.476\,x_L^2\,\mathrm{GeV}^2$. It rises from the lowest x_L due to the increase in p_T^2 space, reaches a maximum near $x_L = 0.6$, and falls to zero at the endpoint $x_L = 1$. The curves show the LO and NLO calculations for the x_L spectrum. They both describe the shape of the spectrum for $x_L > 0.5$, where pion exchange is dominant. The LO calculation also agrees with the normalization of the data, whereas the NLO calculation predicts significantly more neutrons in this range. Neither calculation predicts as many neutrons with $x_L < 0.5$ as observed in the data. A similar failure of exchange models to describe low x_L neutron production has been seen for photoproduction [7].

3 Comparison to neutron production in DIS

Figure 5 compares the leading neutron x_L spectra in dijet photoproduction and DIS [7]. There are significantly fewer neutrons in dijet photoproduction than in DIS. The suppression is negligible for $x_L < 0.4$, and increases with rising x_L to greater than 50% for

$x_L > 0.8$. This pattern is suggestive of kinematic suppression, with the large energy requirement for dijet production in the central ZEUS detector decreasing the phase space available for production of high energy neutrons.

To investigate such kinematic constraints the following quantity is considered:

$$X_{BP} = 1 - \frac{E + P_Z}{2E_p}.$$

Here $E_p = 920\,\text{GeV}$ is the proton beam energy and the quantity $E + P_Z = \sum_i E_i(1 + \cos\theta_i)$, where the sum runs over all calorimeter cells with energy E_i and polar angle θ_i. The quantity X_{BP} is the fraction of the proton beam energy available for particle production into the forward beam pipe, and the energy of leading neutrons is constrained to $x_L < X_{BP}$. The X_{BP} distributions for dijet photoproduction and DIS without a leading neutron requirement are shown in Fig. 6. The dijet photoproduction data are peaked at significantly lower X_{BP} and have a much larger tail at very low X_{BP} than the DIS data. This is qualitatively consistent with the differences in the neutron x_L spectra: the lower X_{BP} values in dijet photoproduction events constrain the neutrons to lower x_L than in DIS.

A quantitative comparison of the kinematic suppression was made by reweighting the neutron x_L spectrum in DIS by the ratio of the inclusive dijet photoproduction to DIS X_{BP} distributions in Fig. 6. The resulting x_L distribution is compared to the the dijet photoproduction data in Fig. 7. The X_{BP}-reweighted DIS x_L distribution gives a fair description of the shape and normalization of the dijet photoproduction data; the differences between the two spectra in Fig. 5 are largely accounted for by the kinematics observed in the central ZEUS detector.

The corrected p_T^2 distributions for different x_L bins are shown in Fig. 8. The line on each plot is a fit to the functional form $d\sigma_{\text{LN}}/dp_T^2 \propto \exp(-bp_T^2)$. The distributions are compatible with a single exponential. The slopes b of the p_T^2 distributions for dijet photoproduction and DIS [7] are compared in Fig. 6. Within the limited statistics of the dijet photoproduction data there is no significant difference between the two sets.

4 Summary

Differential cross sections for dijet photoproduction in association with a leading neutron using the reaction $e^+ + p \to e^+ + n + \text{jet} + \text{jet} + X$ have been measured with the ZEUS detector at HERA using an integrated luminosity of 40 pb^{-1}. The cross sections were measured for jet transverse energies $E_T^{\text{jet 1(jet 2)}} > 7.5(6.5)\,\text{GeV}$ and pseudorapidities ($-1.5 < \eta^{\text{jet}} < 2.5$), photon-proton center-of-mass energy $130 < W < 280\,\text{GeV}$, neutron energy $E_n > 184\,\text{GeV}$, and neutron production angle $\theta_n < 0.75$ mrad. The data are compared to an inclusive sample of dijet events selected without the requirement of a forward neutron. The ratio of leading neutron to inclusive dijet photoproduction was studied as a function of the jet kinematic variables and W and x_γ. The ratios are in fair agreement with the NLO calculation of Klasen and Kramer [15], and therefore consistent with the Regge factorization hypothesis.

To investigate possible absorption effects, the neutron rate and x_L spectra are compared to similar results from DIS. Leading neutrons production in dijet photoproduction is strongly suppressed compared to inclusive DIS. Following a reweighting procedure in the variable X_{BP}, this discrepancy was shown to be mainly due to the different kinematics observed in the central ZEUS detector for dijet photoproduction and DIS. No clear absorption effects were seen.

The similarity of the neutron yields and x_L and p_T distributions in dijet photoproduction and DIS, after accounting for kinematics observed in the central ZEUS detector, indicates the same mechanism for neutron production in both processes.

References

[1] ZEUS Coll., M. Derrick et al., Phys. Lett. **B 384**, 388 (1995).

[2] H1 Coll., C. Adloff et al., Eur. Phys. J. **C 6**, 587 (1999).

[3] ZEUS Coll., J. Breitweg et al., Nucl. Phys. **B 596**, 3 (2001).

[4] ZEUS Coll., S. Chekanov et al., Nucl. Phys. **B 637**, 3 (2002).

[5] ZEUS Coll., S. Chekanov et al., Nucl. Phys. **B 658**, 3 (2003).

[6] ZEUS Coll., S. Chekanov et al., Phys. Lett. **B 590**, 143 (2004).

[7] ZEUS Coll, S. Chekanov et al., Nucl. Phys. **B 776**, 1 (2007).

[8] H. Yukawa, Proc. Phys. Math. Soc. Japan **17**, 48 (1935).

[9] J. D. Sullivan, Phys. Rev. D **5**, 1732 (1972).

[10] M. Bishari, Phys. Lett. B **38**, 510 (1972).

[11] S. N. Ganguli and D. P. Roy, Phys. Rep. **67**, 201 (1980).

[12] V. R. Zoller, Z. Phys. C **53**, 443 (1992).

[13] A.B.Kaidalov et al., European Physics Journal **C47**, 386 (2006).

[14] V.A. Khoze, A.D. Martin and M.G. Ryskin, Preprint IPPP-06-36, DCPT-06-72 (hep-ph/0606213), 2006.

[15] M. Klasen, G. Kramer, Eur. Phys. J. **C49**, 957 (2007).

[16] H. Holtmann et al., Phys. Rev. Lett. B **338**, 363 (1994).

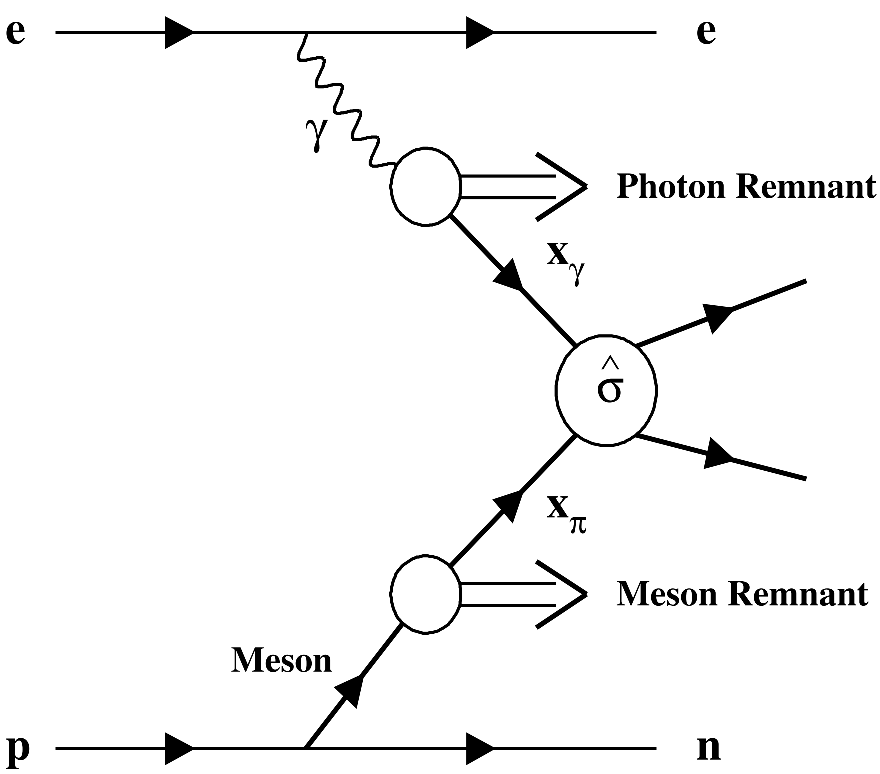

Figure 1: *Resolved photoproduction of dijet events with a leading neutron through meson exchange. The fraction of the energy of the exchanged meson (photon) participating in the partonic hard scattering that produces the dijet system is denoted by x_π (x_γ); the corresponding hard cross section is $\hat{\sigma}_{\gamma\pi}$. In direct photoproduction, the entire exchanged photon participates in the hard scattering, there is no photon remnant, and $x_\gamma = 1$.*

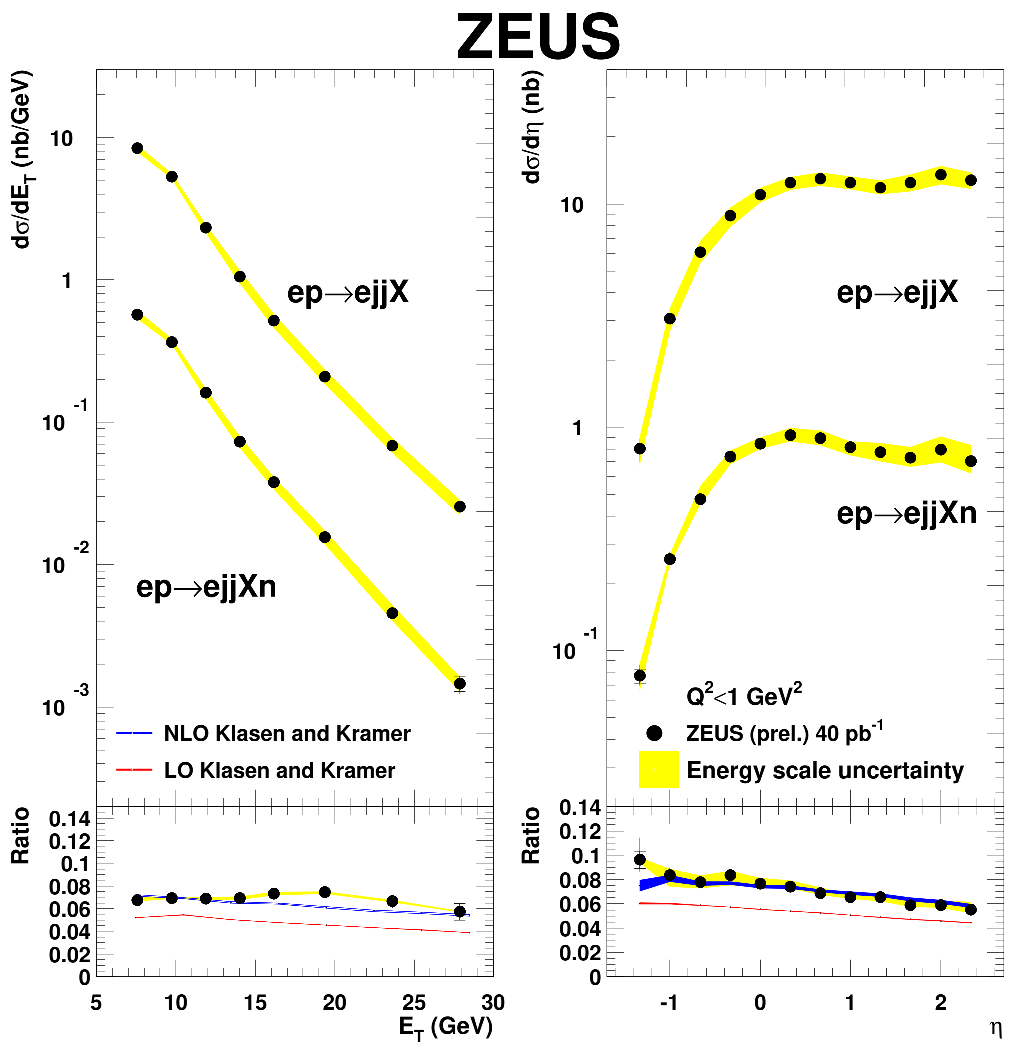

Figure 2: *The differential dijet cross sections as a function of $E_T^{\rm jet}$ and η for dijet photoproduction and neutron-tagged dijet photoproduction (top), and the ratio between them (bottom). The kinematic region measured is $E_T^{\rm jet\ 1(jet\ 2)} > 7.5(6.5)\ GeV$, $-1.5 < \eta^{\rm jet} < 2.5$, $Q^2 < 1\ \ GeV^2$, $130 < W < 280\ GeV$ for both samples, with the additional restriction of $x_L > 0.2$ and $\theta_n < 0.75$ mrad for the neutron-tagged sample. The ratios of the cross sections are compared to the predictions of Klasen and Kramer [15]. The calculations are at the parton level; effects of hadronization are expected to cancel in the ratio. The statistical and systematic errors are summed in quadrature; the calorimeter energy scale uncertainty is shown separately as a yellow band.*

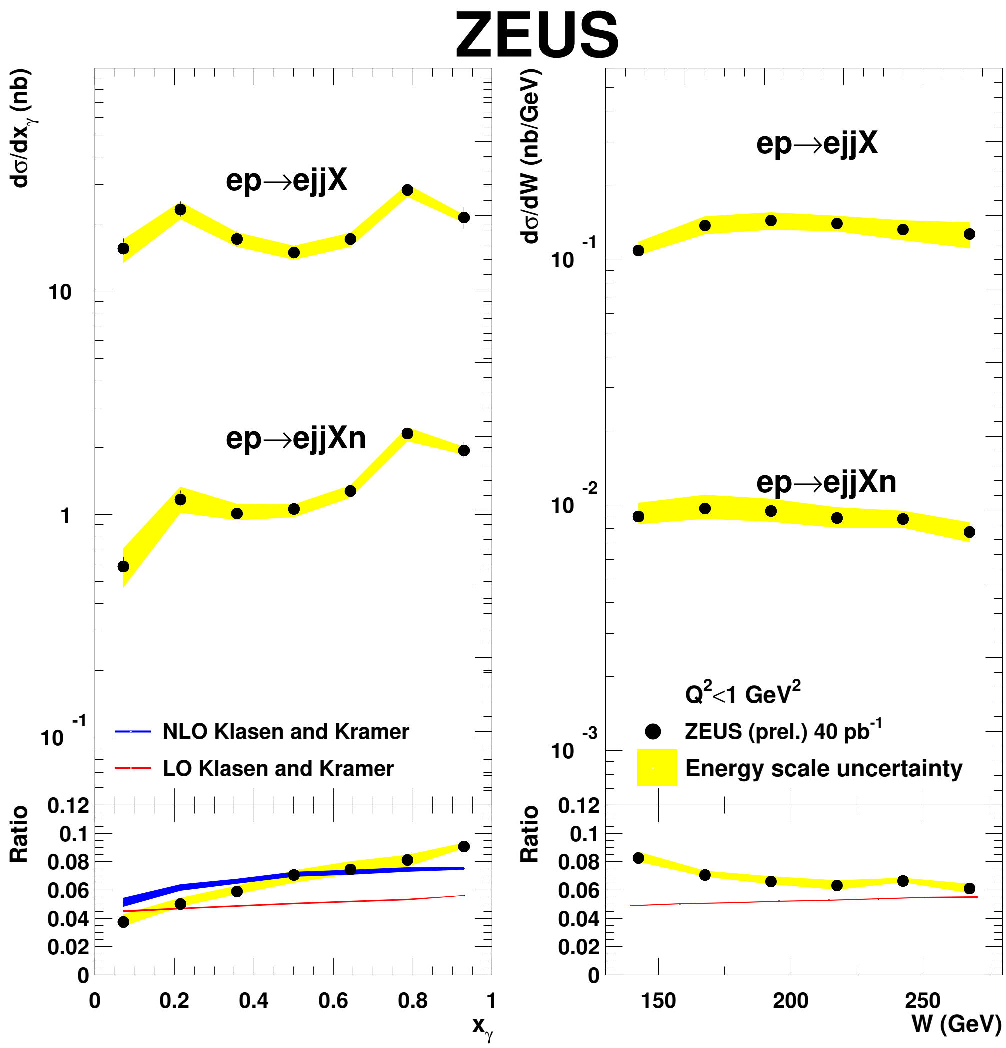

Figure 3: *The differential dijet cross sections as a function of x_γ and W (top) and the ratio between them (bottom), measured in the same kinematic region as in Fig. 2. The ratios of the cross sections are compared to the predictions of Klasen and Kramer [15].*

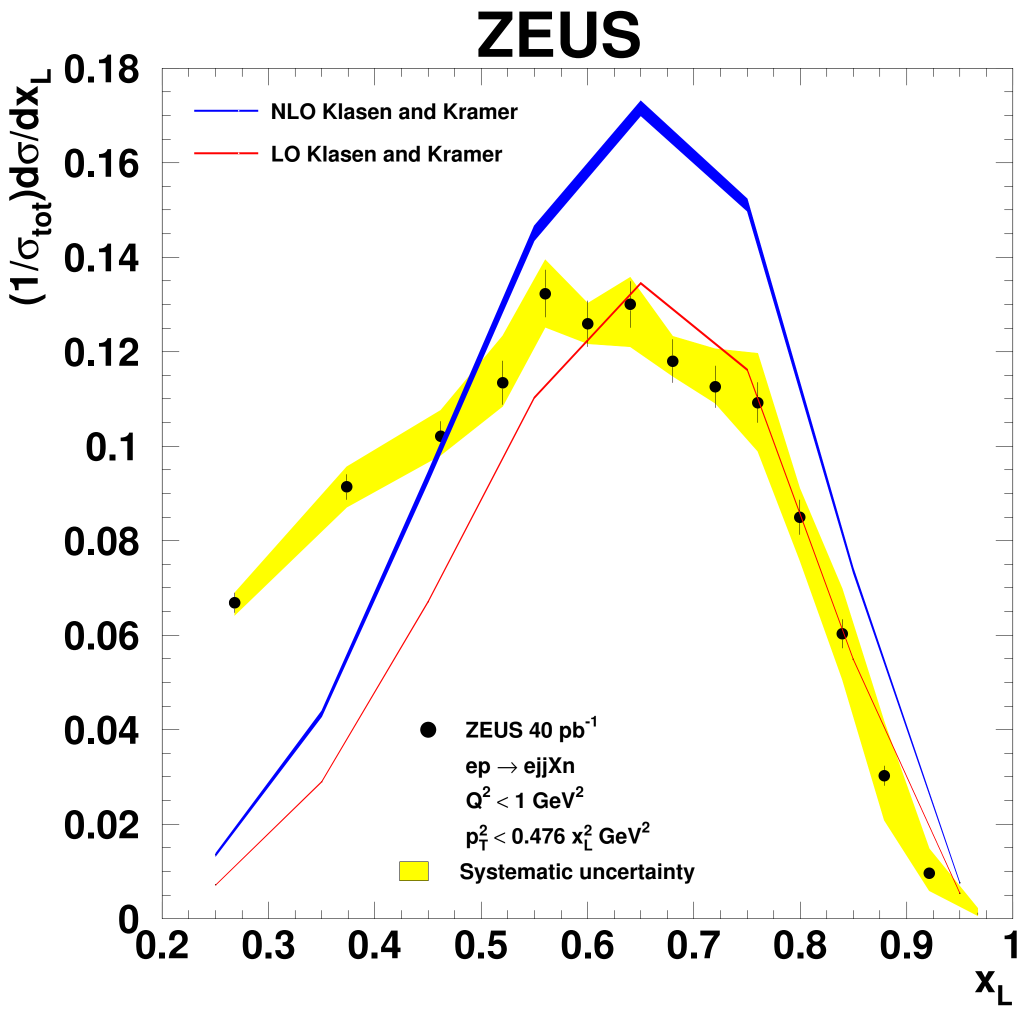

Figure 4: *The normalized differential distribution* $(1/\sigma_{\rm inc})d\sigma_{LN}/dx_L$ *for dijet events. The curves are the LO and NLO calculations of Klasen and Kramer [15].*

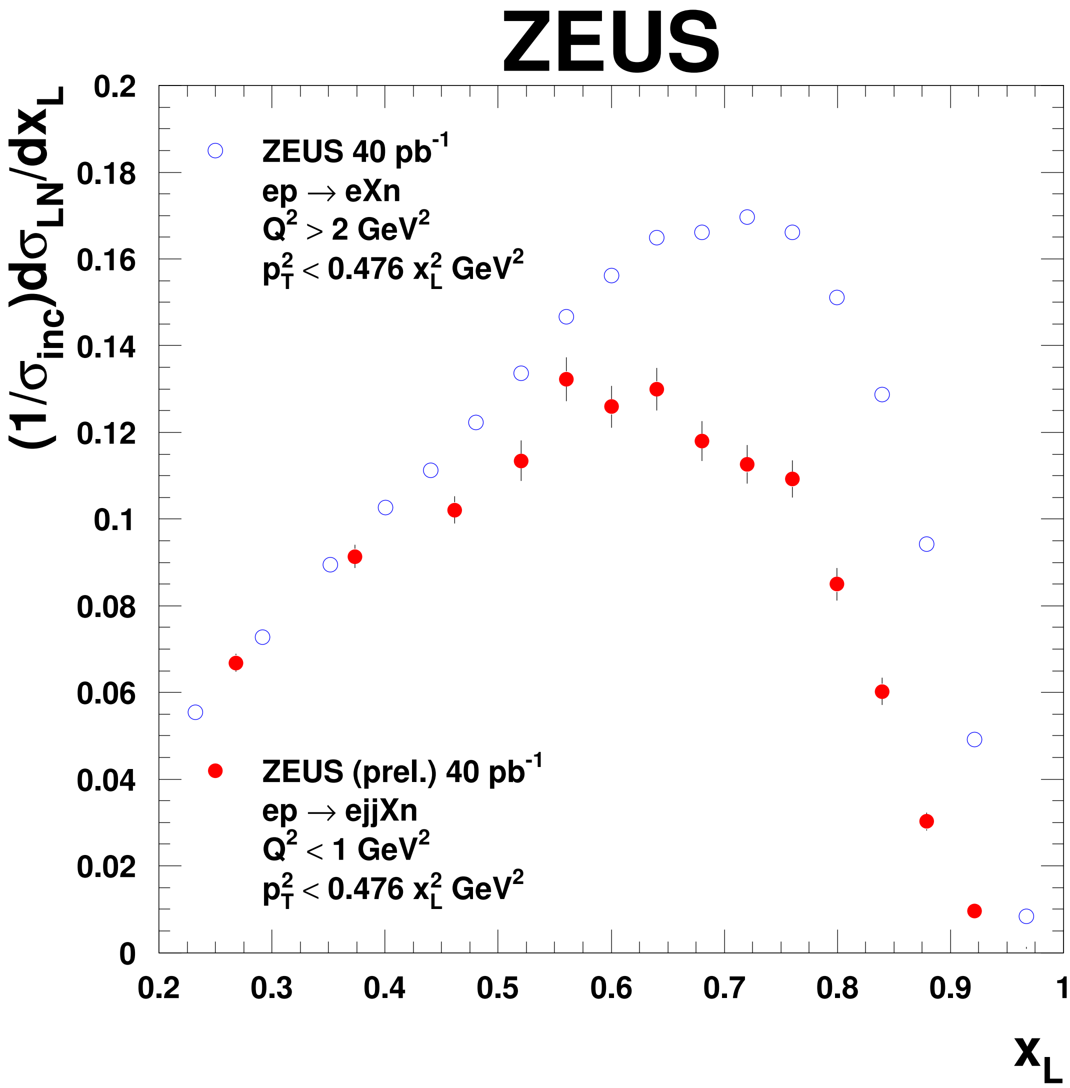

Figure 5: *The distribution $(1/\sigma_{inc})d\sigma_{\rm LN}/dx_L$ for neutrons with scattering angles $\theta_n < 0.75$ mrad, corresponding to the kinematic range $p_T^2 < 0.476\, x_L^2$ GeV^2. The solid points are for dijet photoproduction, the open points for DIS [7]. The error bars show the statistical uncertainties.*

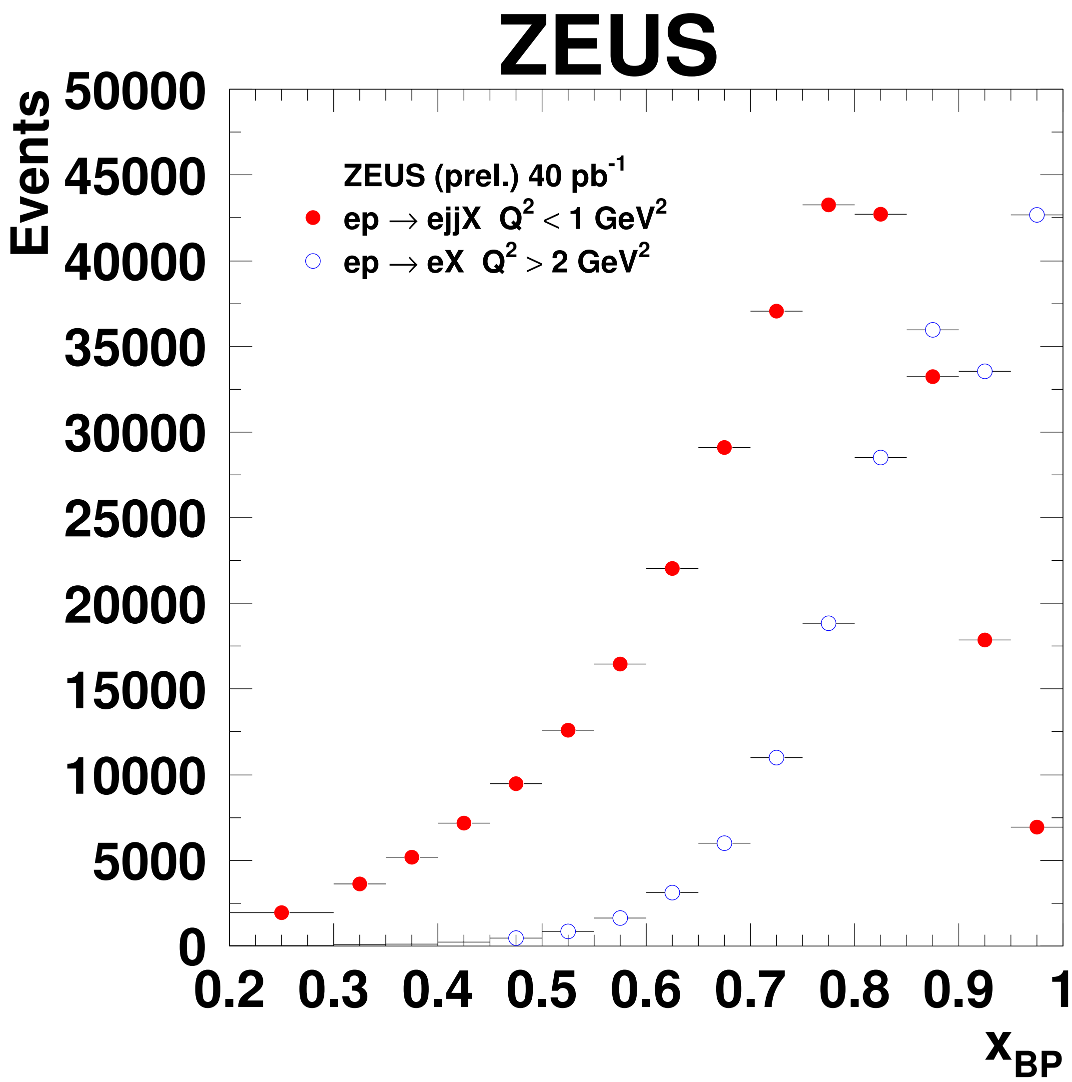

Figure 6: *Histogram of the quantity X_{BP} described in the text for events in dijet photoproduction and DIS without the neutron requirement.*

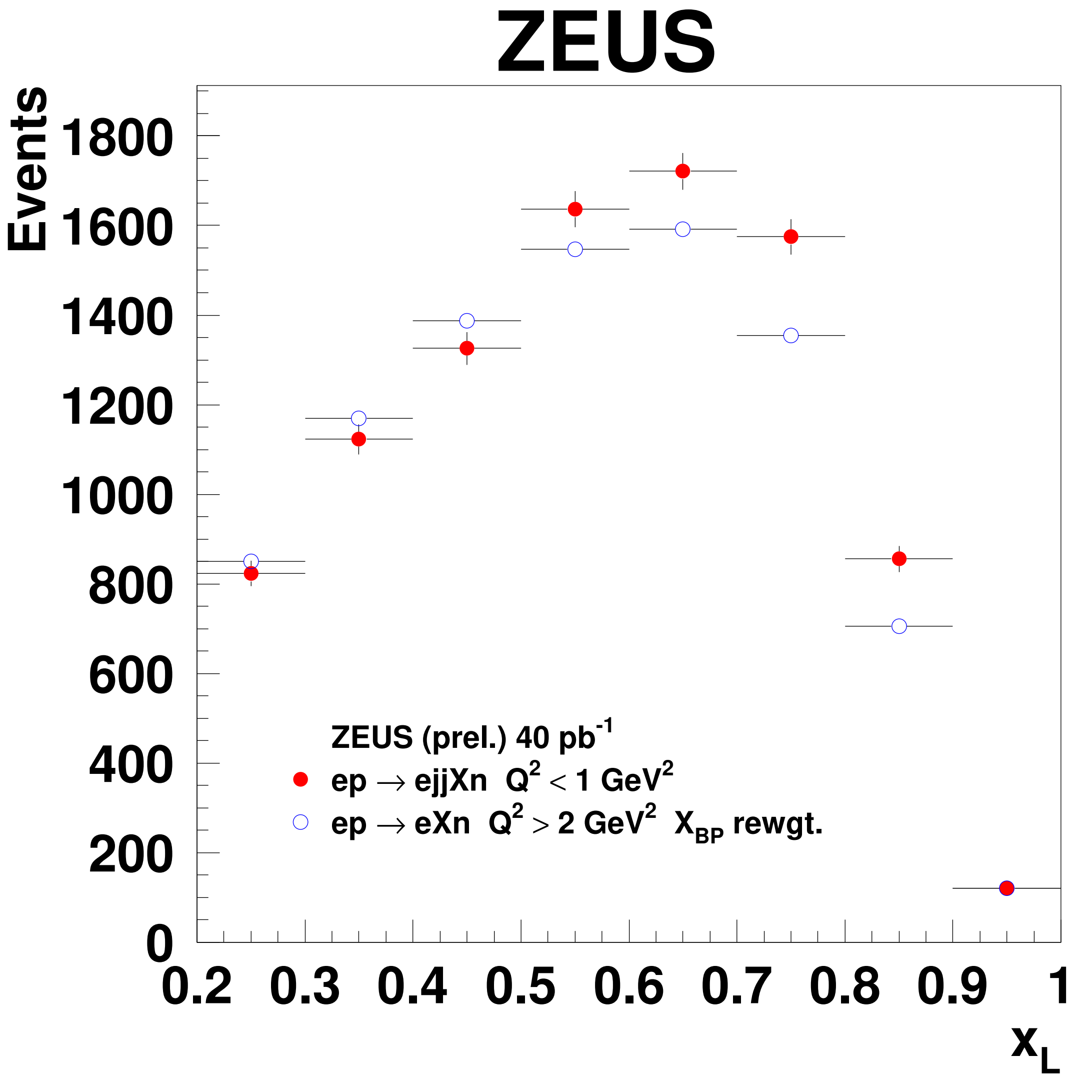

Figure 7: *The solid points are a histogram of x_L for leading neutrons in dijet photoproduction. The solid histogram is the same for leading neutrons in DIS, rewighted as a function of X_{BP} as described in the text.*

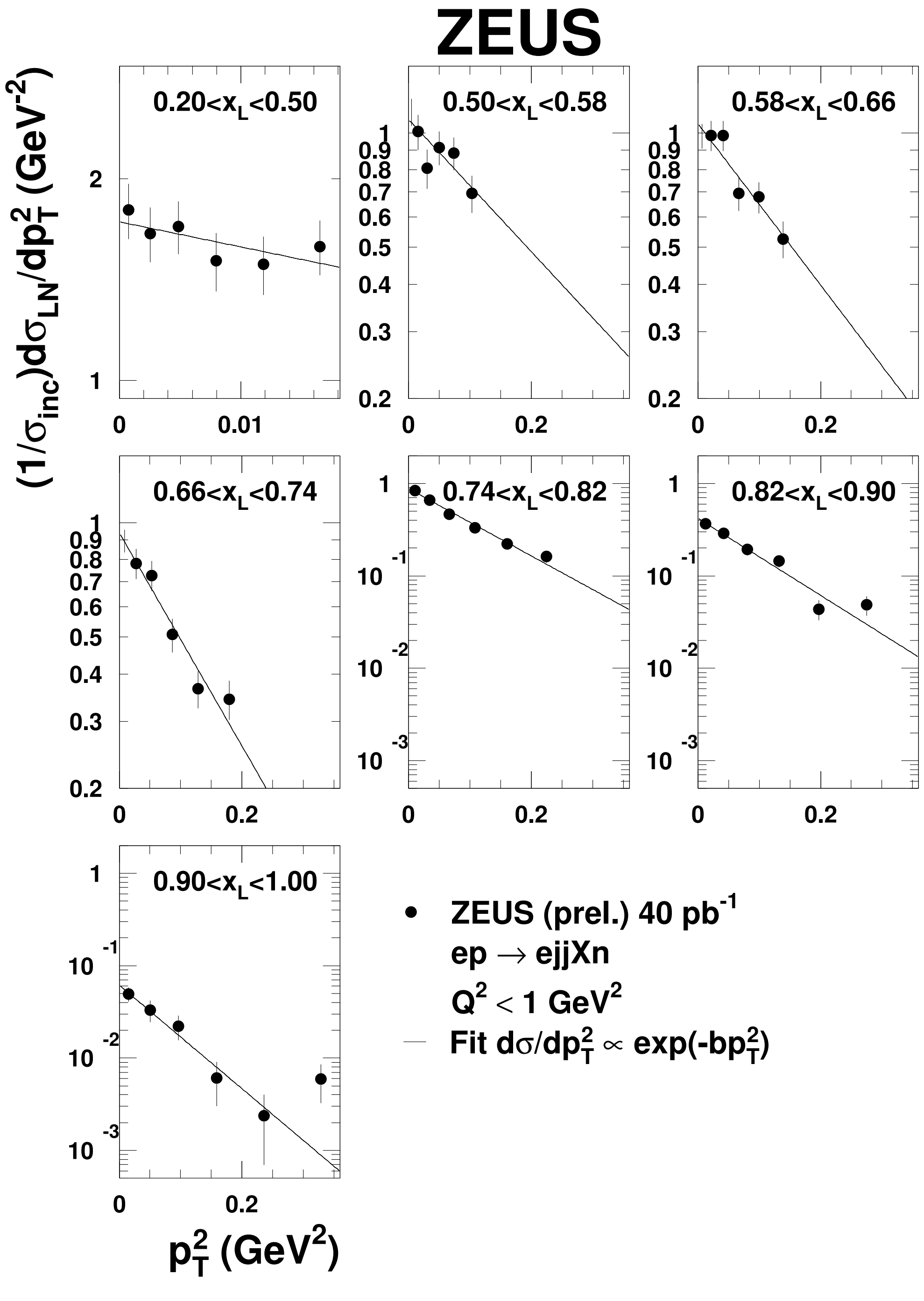

Figure 8: *The doubly differential distributions* $(1/\sigma_{\rm inc})d^2\sigma_{\rm LN}/dx_L dp_T^2$ *in bins of* x_L*. Note the logarithmic vertical scale and the smaller* p_T^2 *range for the lowest* x_L *bin. The statistical uncertainties are shown by a vertical error bar. The line on each plot is the result of a fit to the form* $d\sigma_{\rm LN}/dp_T^2 \propto \exp(-bp_T^2)$*.*

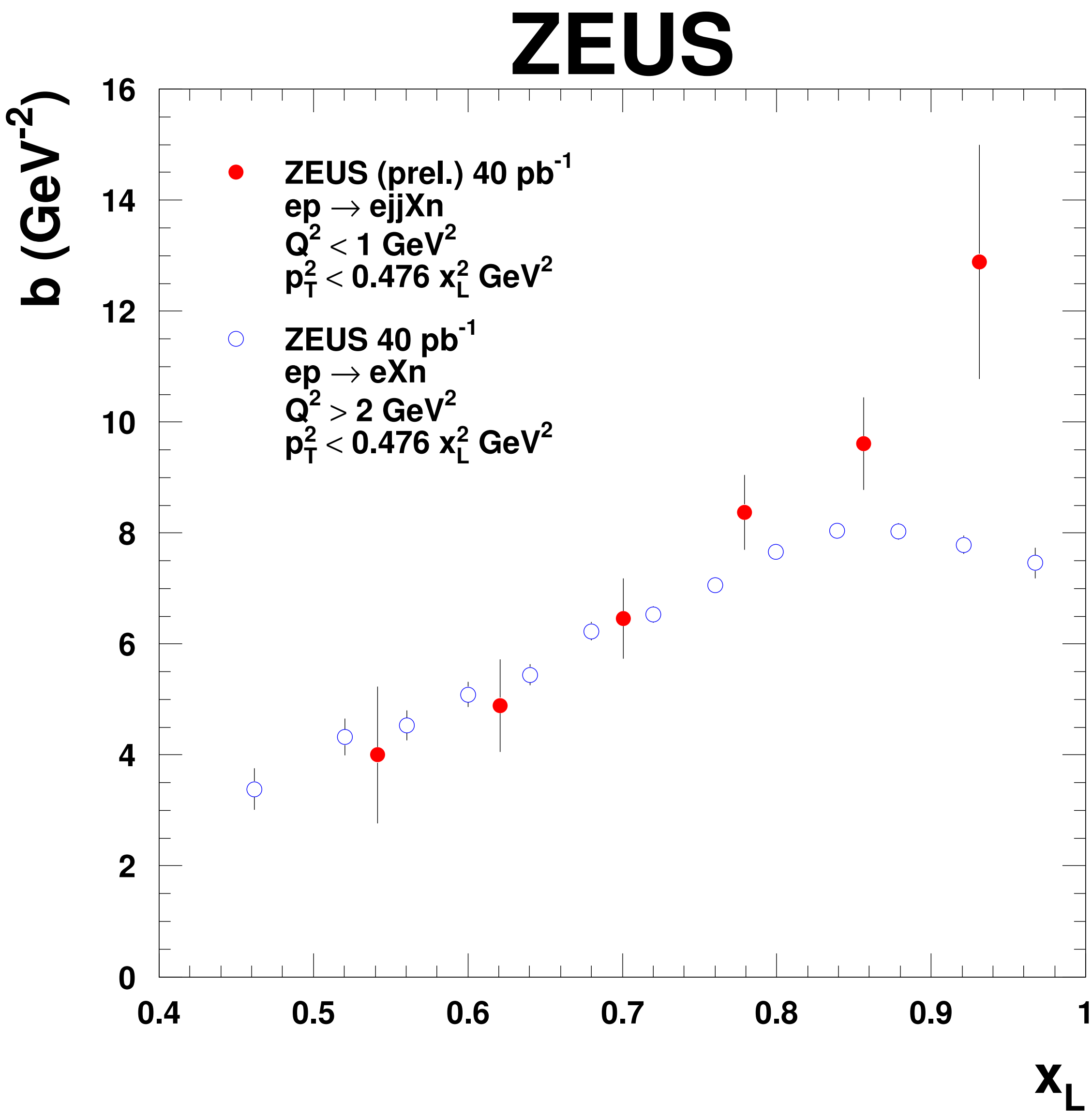

Figure 9: *The exponential slopes b versus x_L from fits of the p_T^2 distributions to the form $d\sigma_{\rm LN}/dp_T^2 \propto \exp(-bp_T^2)$ over the range $p_T^2 < 0.476\, x_L^2$ GeV^2. The solid points are for dijet photoproduction, the open points for DIS [7]. The error bars show the statistical uncertainties.*